Real-Time Localized Control of Transient Stability with Static Synchronous Series Compensator (SSSC)

Invited Paper

Abdul M. Miah
Department of Industrial & Electrical Engineering Technology, South Carolina State University, Orangeburg, South Carolina, USA
Email: amiah@scsu.edu

***Abstract*—Very recently, a new transient stability methodology referred to as the Localized Transient Stability (LTS) Method was proposed solely for the purpose of real-time localized control of transient stability. The method is based on a completely new idea of localized transient stability. In this paper, real-time localized control of transient stability by the LTS method is described. Since the technique is based on the LTS method, transient stability in this technique is viewed as the interaction of each individual generator with its respective remaining generators. Therefore, in this technique, the post-fault power system is represented by a two-generator localized power system at the site of each individual generator. Each of these localized power systems is then driven to its respective stable equilibrium by local control actions with local computations using the locally measured data in order to drive the full (entire) power system to its stable equilibrium. New investigative results are presented with Static Synchronous Series Compensator (SSSC) as the local control means to demonstrate the potential of real-time localized control of transient stability by the LTS method.**

***Index Terms*—localized power system, localized transient stability, real-time localized control, transient stability**

I. Introduction

Transient stability assessment and control are crucial for the secured operation of power systems. In the context of on-line applications, a number of computationally fast transient stability assessment methods have been reported in the literature. Among these, the direct methods such as the transient energy function method [1] and Extended Equal Area Criterion (EEAC) [2] are the important ones which have been implemented at some utility companies [3]. However, all the fast methods use classical representation of power systems and hence they are limited to short term assessment like the first swing stability. All these fast methods are faster than the standard Step-by-Step (SBS) numerical integration method which is considered as the most accurate method of transient stability assessment since this method can accommodate any degree of modeling of the power systems. The fast methods can be made even faster by coupling with them the dynamic equivalent reduction techniques [4]-[6]. Some recent developments in transient stability assessment have been reported in [7]-[12]. There are also research efforts in using parallel processing [13]-[15] to speed up the time-domain transient stability simulations.

Besides the natural causes (hurricane, tornado, ice storm, earthquake, etc.), transient instability has been known to be a major cause for widespread power blackouts. Power blackout does not occur frequently, but when it does, the impacts can be devastating in terms of human sufferings and financial losses. Since a vast majority of U.S. agricultural farms rely on the electricity from power grids for their proper operation, power blackouts can have disastrous effects in terms of significant losses of crops and livestock. Power blackouts can also cause substantial spoilage of refrigerated agricultural products. In addition, power blackouts can have serious impacts in terms of huge financial losses by the other businesses. Therefore, with the stressed transmission systems of today, real-time control of transient stability is critically important to avoid widespread power blackouts due to transient instability. However, all the transient stability methods require system-wide transfer of measurement data to the system control center for use in real-time control of transient stability. Due to the development of Phasor Measurement Unit (PMU), there are research efforts for real-time transient stability assessment [16]-[19] using PMU measurements. There are also research efforts for real-time centralized control of transient stability [19]-[21] using control actions like tripping of generators, tripping of transmission lines, etc.

However, since real-time localized control of transient stability can be much simpler, faster and cheaper compared to the real-time centralized control, there are research efforts for localized controls. These localized controls use local computations with local information and measurements. To avoid the system-wide transfer of real-time measurement data, Local Equilibrium Frame (LEF) was suggested in [22] for the purpose of localized

Manuscript received August 9, 2018; revised August 25, 2018, accepted September 13, 2018.
Corresponding author: Abdul M. Miah (email: amiah@scsu.edu)

doi: 10.18178/ijeetc.8.1.1-8

control. However, the equilibrium state in LEF refers to a state at which all the generators run at synchronous speed. This synchronous speed equilibrium condition is sufficient, but not necessary, as it is too restrictive. This is a serious drawback of LEF. The Center-of-Angle (COA) frame of reference in which the generator angles are with respect to the center of angles of all the generators, and the machine frame of reference in which the generator angles are with respect to the angle of a chosen common generator do not suffer from such drawback. The equilibrium state in these reference frames refers to a state at which all the generators run at the same speed that is not necessarily the synchronous speed. Further, LEF cannot provide any dynamic equation for the external system. This is another drawback of LEF. There are also a number of strategies [23]-[28] that have been suggested in the literature for localized control of transient stability using different control means like braking resistors, series capacitors, fast valving and Flexible Alternating Current Transmission System (FACTS) devices. However, these strategies are developed using very simplified models for the external systems like the infinite bus. Therefore, in each of these strategies, equilibrium refers to synchronous speed equilibrium which is a serious drawback. A control strategy based on simplified model may work only for some special faults in a multi-machine power system [27]. In all these strategies, simplified models are used due to the lack of availability of a suitable dynamic model for the remaining generators and a methodology that can be implemented for localized control of transient stability in multi-machine power systems.

To overcome the drawbacks of localized control, a new methodology referred to as the Localized Transient Stability (LTS) Method [29]-[32] was very recently proposed solely for the purpose of real-time localized control of transient stability. However, the details of the mathematical formulations of the LTS method have been presented in [30]. This LTS method is based on localized transient stability of a power system. This is completely a new idea. The method can be easily implemented for real-time localized control of transient stability. The system equilibrium state in the LTS method refers to a state at which all the generators run at the same speed that is not necessarily the synchronous speed. The method also provides dynamic equations for the remaining generators, which are necessary to design effective localized control strategies that can drive the power system to its appropriate equilibrium. In this present paper, some new investigative results with Static Synchronous Series Compensator (SSSC) as the local control means are presented to demonstrate the potential of the real-time localized control of transient stability by the LTS method. This investigation was carried out on the very well-known New England 39-bus 10-generator system.

II. Localized Transient Stability (LTS) Method

The details of the mathematical formulations of the LTS method have been presented in [30]. Here, the LTS method is described briefly. In the LTS method, transient stability is viewed as the interaction of each individual generator with its respective remaining generators. Therefore, the method uses two-generator localized models of the power system as it is viewed at the sites of different individual generators. To develop this localized power system (LPS) model, a simple dynamic equivalent has been developed for the remaining generators which may or may not be coherent. Therefore, this dynamic equivalent is different from the coherency-based dynamic equivalents. This dynamic equivalent is obtained by satisfying the necessary nodal equation and generator swing equations. However, in the presence of a fault like the short circuit fault on the system, this dynamic equivalent is not available. Therefore, the LTS method uses the post-fault system. Note that the transient stability assessment and control is actually the assessment and control of the post-fault system. In this presentation, a power system of n generators with classical representation is considered. The post-fault power system network at the site of an individual generator, say the nth generator also referred to as the local generator, is partitioned into two subsystems at the internal bus of the local generator: subsystem C containing the local generator, and subsystem D containing the remaining system. These two subsystems are connected to each other only at the internal bus of the local generator. The following sets of indices are defined:

$$C_I = \{n\};\ D_I = \{1,\ 2,\ \cdots,\ (n-1)\}$$

where C_I is the index for the local generator internal bus, and D_I are the indices for all the $(n-1)$ remaining generator internal buses.

A. A Simple Single-Generator Dynamic Equivalent for the Remaining Generators

The details of the mathematical development of this dynamic equivalent has been presented in [30]. Here, it is described briefly. This dynamic equivalent satisfies the nodal equation at the local generator internal bus and $(n-1)$ swing equations of the remaining generators.

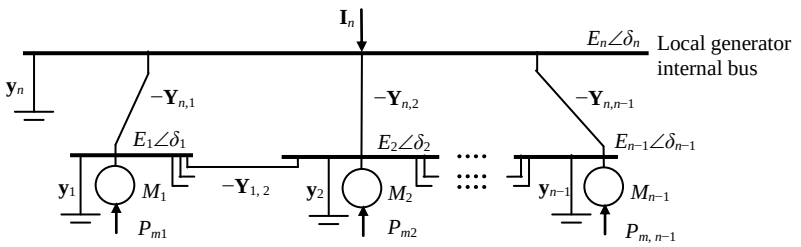

Fig. 1. Remaining system D (the power system external to the local generator internal bus)

After the power system network is reduced to the generator internal buses, the power system external to the local generator internal bus appears as shown in Fig. 1. Here, $\mathbf{I}_n$=phasor current injected into area D at the local generator internal bus, $\mathbf{y}_k$ is a shunt admittance at an internal bus k that appears due to network reduction, $\mathbf{Y}_{ik}=\mathbf{Y}_{ki}=G_{ik}+jB_{ik}=G_{ki}+jB_{ki}$=elements of the reduced admittance matrix of the power system network, and $\mathbf{E}_i=E_i\angle\delta_i$ = phasor voltage of a generator internal bus. Further, M_i, δ_i and P_{mi} are respectively the inertia constant, rotor angle and mechanical input power of a generator. However, from the electrical network point of view, only the network shown in Fig. 2 (a) is seen by the local generator internal bus. Therefore, to satisfy the dynamic behavior of a remaining generator i in Fig. 2 (a), an equivalent mechanical input power P_i is defined for this generator using some mathematical manipulation. This P_i as shown in Fig. 2 (a) produces the original post-fault trajectory of this generator. However, this mathematical manipulation makes P_i a time varying quantity unless all the remaining generators are coherent.

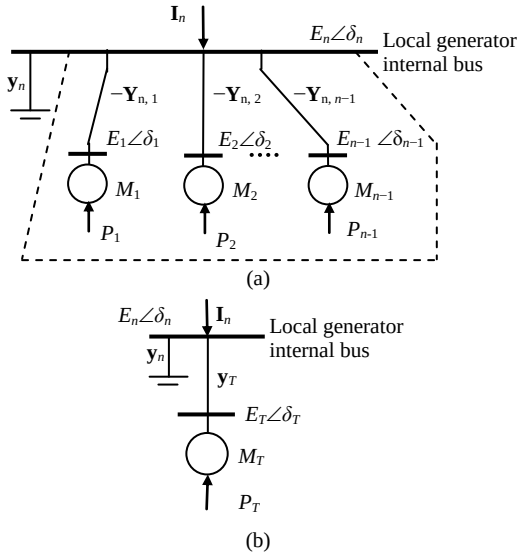

Fig. 2. Equivalent systems: (a) Equivalent of remaining system D as seen by the local generator and (b) single-generator dynamic equivalent of remaining system D

To aggregate the generators of Fig. 2 (a) to one equivalent generator, the shunt admittance $\mathbf{y}_n$ that appears at the local generator internal bus due to network reduction is retained, and the network enclosed by the dashed lines is replaced by its Thevenin equivalent consisting of a voltage source having the phasor voltage of $\mathbf{E}_T$ in series with an admittance of $\mathbf{y}_T$. Therefore, Fig. 2 (b) now becomes the single-generator dynamic equivalent of Fig. 2(a). In Fig. 2 (b), E_T, δ_T, M_T, and P_T are respectively the internal bus voltage magnitude, rotor angle, inertia constant, and mechanical input power of the equivalent generator. Further, the admittances $\mathbf{y}_n$ and $\mathbf{y}_T$ are respectively given by

$$\mathbf{y}_n = \mathbf{Y}_{nn} + \sum_{k\in D_I} \mathbf{Y}_{nk} \tag{1}$$

$$\mathbf{y}_T = (g_T + jb_T) = -\sum_{k\in D_I} \mathbf{Y}_{nk} = -\sum_{k\in D_I} \mathbf{Y}_{kn} \tag{2}$$

The inertia constant M_T and mechanical input power P_T of the equivalent generator are given by

$$M_T = \sum_{i\in D_I} M_i, \qquad P_T = \sum_{i\in D_I} P_i \tag{3}$$

where M_i and P_i are respectively the inertia constant and the equivalent mechanical input power of a remaining generator. Further, $\mathbf{E}_T$ is given by

$$\mathbf{E}_T = E_T\angle\delta_T = (\sum_{k\in D_I} \mathbf{Y}_{nk}\mathbf{E}_k)/(\sum_{k\in D_I} \mathbf{Y}_{nk}) \tag{4}$$

Equation (4) clearly indicates that $\mathbf{E}_T$ is an admittance-weighted aggregated average phasor voltage of all the remaining generator internal bus phasor voltages. Thus the angle of this aggregated average phasor voltage is taken as the rotor angle δ_T. Using (4), it can be shown that E_T is a time varying quantity unless all the remaining generators are coherent.

B. Post-Fault Localized Power System Model

The power system as seen at the site of the nth local generator now consists of the subsystem C and the dynamic equivalent of Fig. 2 (b). Therefore, the localized power system (LPS) model takes the form shown in Fig. 3. Here, δ_n, M_n, and P_{mn} are respectively the rotor angle, inertia constant, and mechanical input power of the local generator. Again, δ_T, M_T, and P_T are respectively the rotor angle, inertia constant, and mechanical input power of the equivalent generator.

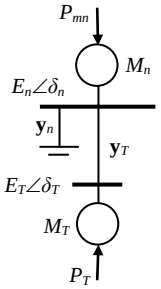

Fig. 3. Localized power system (LPS) model at the site of nth generator.

The dynamics of the localized two-generator power system of Fig. 3 can be put in the familiar two-state form of representation as

$$\omega = \dot{\delta} = \omega_n - \omega_T \tag{5a}$$

$$\dot{\omega} = M_n^{-1}\left(P_{mn} - P_{en}\right) - M_T^{-1}\left(P_T - P_{eT}\right) \tag{5b}$$

where $\delta = \delta_n - \delta_T$, and P_{en} and P_{eT} are respectively the electrical output powers of the local generator and the equivalent generator. Here, δ and ω are the state variables of the LPS and they respectively represent the separation angle and speed of the individual generator from its respective remaining generators. Further, ω_n and ω_T are respectively the speeds of the local generator and the equivalent generator. The two-generator localized power system described by (5) is referred to as the nth localized power system.

Consider that the full power system after a major disturbance reaches its appropriate stable equilibrium

point in the post-fault configuration. Then all the generators are coherent, i.e. they operate at the same speed which is not necessarily the synchronous speed. Under this condition, it can be shown mathematically that each of the localized power systems also reaches its respective stable equilibrium point. In other words, it can be said that if each of the localized power systems reaches its respective stable equilibrium, then the full system is in appropriate stable equilibrium. This is the basis of the proposed transient stability method. This basis is also supported by the investigative test results. Further, since the LTS method involves each of the LPS trajectories, it captures all the transient stability phenomena of the full system. This is also supported by the test results based on the comparison of Critical Clearing Time (CCT) by the LTS method with that by the SBS method. However, as discussed in [29], the LTS method is not at all intended for transient stability assessment. It is intended solely for the real-time localized control of transient stability.

Therefore, in terms of control of transient stability by the LTS method, if each of the localized power systems is driven by local control actions to its respective stable equilibrium, then the full power system is driven to its stable equilibrium. Note that the two-generator localized model at the site of a local generator describes the dynamic behavior of the entire power system as viewed at the site of the local generator. Therefore, these localized power system models are not subsystems like the interconnected subsystems in a power system where the entire power system can be unstable even though each subsystem is stable.

C. Real-Time Localized Control of Transient Stability by the LTS Method

The real-time localized control of transient stability by the LTS method is described here. In terms of localized control, if each LPS is driven to its respective stable equilibrium i.e. if each LPS trajectory is stabilized by local control actions, then the full system is driven to its stable equilibrium. However, to apply the LTS method, as described in [29], it is essential that the local control actions (if any) at different generator sites are applied during the same time step such that there is no local control action present in the power system at the beginning of any particular time step. This is necessary to ensure that the post-fault power system returns to the original post-fault system at the beginning of any particular time step. Therefore, it is assumed that each generator site uses the fault clearing time as a common reference time so that the beginning and ending of the time steps used by each generator site are same. As such, the post-fault power system returns to the original post-fault system at the beginning of each time step. At the beginning of a particular time step, necessary local computations are done independently at each local generator site using the same original post-fault passive network model. However, the necessary local control actions (if any) at different generator sites are applied during the same time step. Note that the different local control means including the FACTS devices can be easily integrated into the network model of the local generator site for the purpose of control.

Consider the *n*th LPS. With the known passive network model of the pre-fault power system and fault information, the admittance matrix of the LPS and hence the admittance parameters $\mathbf{y}_n$ and $\mathbf{y}_T$ of the LPS model can be obtained easily. Then with the known total inertia constant (M_T) of the remaining generators, all the unknown variables of the LPS can be estimated from real-time measurement data taken solely at the *n*th local generator and the local information as discussed here. With known resistance and direct axis transient reactance of the *n*th local generator, voltage E_n, real power P_{en}, and the reactive power Q_{en} at the internal bus can be determined using measurement data like the real power, reactive power, and voltage magnitude taken at its external bus. However, P_{en} and Q_{en} in terms of the LPS quantities are given by

$$P_{en} = E_n^2 G'_{n,n} + E_n E_T [G'_{n,T} \cos\delta + B'_{n,T} \sin\delta] \quad (6a)$$

$$Q_{en} = -E_n^2 B'_{n,n} + E_n E_T [G'_{n,T} \sin\delta - B'_{n,T} \cos\delta] \quad (6b)$$

Here, ($G'_{n,n} + j\,B'_{n,n}$) and ($G'_{n,T} + j\,B'_{n,T}$) are two elements of the admittance matrix of LPS shown in Fig. 3. Equations (6) can be solved to yield

$$\delta = \tan^{-1}[(Q_{en} + E_n^2 B'_{n,n})/(P_{en} - E_n^2 G'_{n,n})] + \beta \quad (7)$$

where $\beta = \tan^{-1}(B'_{n,T} / G'_{n,T})$.

So, the LPS angle δ can be determined by (7) with P_{en} and Q_{en} obtained from measurement data. However, the angle δ obtained from (7) must be adjusted by the addition or subtraction of an integer number times 2π electrical radians for pole slippage to obtain the LPS angular trajectory corresponding to the local generator. Therefore, the LPS angle δ can be determined by (7) with proper adjustment of δ as indicated. With known values of δ at some suitable time steps, δ can be approximated by a third degree polynomial and then both ω and $\dot{\omega}$ can be estimated from its derivatives. E_T can be obtained from (6) as

$$E_T = (1/E_n)\sqrt{\frac{[(P_{en} - E_n^2 G'_{n,n})^2 + (Q_{en} + E_n^2 B'_{n,n})^2]/}{(G'^2_{n,T} + B'^2_{n,T})}} \quad (8)$$

P_{mn} can be obtained from the pre-fault steady-state real power P_{en} since they are equal. P_{eT} can be obtained as

$$P_{eT} = E_T^2 G'_{T,T} + E_T E_n [G'_{T,n} \cos\delta - B'_{T,n} \sin\delta] \quad (9)$$

in terms of LPS quantities. Here, $G'_{n,n}$, $G'_{n,T}$, $G'_{T,T}$, and $G'_{T,n}$ are elements of the conductance matrix of LPS. Further, $B'_{n,n}$, $B'_{n,T}$, and $B'_{T,n}$ are three elements of the susceptance matrix of LPS. With the value of $\dot{\omega}$ estimated from polynomial approximation of δ, P_T can now be estimated from (5b) as

$$P_T = (M_T / M_n)(P_{mn} - P_{en}) - \dot{\omega} M_T + P_{eT} \quad (10)$$

It can be seen here that with the known post-fault passive network model of the power system and the total inertia constant of the remaining generators, all the unknown variables (E_T, δ and P_T) of the LPS model shown in Fig. 3 can be computed from real-time measurement data taken solely at the external bus of the local generator. Therefore, this LPS model can be used to design and implement real-time localized control strategies that can drive the LPS to its stable equilibrium. However, to apply the LTS method, the latest updated pre-fault passive network model of the power system, the fault information including the fault clearing time, and the total inertia constant of the remaining generators must be known at the site of each generator. All these information can be easily obtained from the system control center.

At any instant of time, a stable equilibrium point of the LPS described by (5) can be defined by holding E_T and P_T fixed at their current estimated values. This stable equilibrium state (δ_e, 0) is referred to as the instantaneous stable equilibrium state. Here, δ_e is the instantaneous stable LPS angle that can be obtained from (5b) by setting its left side equal to zero and using (6a) and (9). However, if the values of E_T and P_T sustain, the instantaneous stable equilibrium becomes the stable equilibrium of the LPS. Note that since E_T and P_T are held fixed, δ_e is also fixed i.e. $\dot{\delta}_e$ is zero. In terms of control, if each of the localized power systems is driven to the instantaneous stable equilibrium point of its respective state-space, then the full system is driven to its stable equilibrium. Therefore, the technique can be easily implemented at the site of each local generator independently without requiring any coordination.

III. Test Results

The potential of the real-time localized control of transient stability by the LTS method was investigated on the well-known New England 39-bus 10-generator system. In this investigation, Static Synchronous Series Compensator (SSSC) was used as the local control means. A number of three-phase short circuit faults were considered. These results on real-time localized control of transient stability are presented here. In this investigation, local computations with SBS simulated local measurement data were used to compute the necessary local controls. These local controls were then applied to improve the CCT ranges. In all the SBS simulations, a time-step size of 0.01 s has been used. However, to determine the local controls required to drive the localized power systems to their respective equilibriums i.e. to stabilize the LPS trajectories, optimal aim control strategy [33] was chosen due to its suitability for two-generator systems. With reference to local control of power systems, this optimal aim strategy (OAS) was described in detail in [23] where this strategy was referred to as a Localized Aiming Strategy (LAS). With respect to a two-generator system, this strategy has also been described in [34].

For the purpose of localized control by LTS method using the OAS, the control dependent dynamic equations of the nth localized power system are written in the form as

$$\omega = \dot{\delta}, \quad \dot{\omega} = \left[P_m - P_e + U_n(t)\right]/M \tag{11}$$

where

$$M = M_n M_T /(M_n + M_T),$$
$$P_m = (P_{mn} M_T - M_n P_T)/(M_n + M_T)$$
$$P_e = (P_{en} M_T - M_n P_{eT})/(M_n + M_T) = f(\delta)$$

Here, $U_n(t)$ represents an additive power control in the localized power system. However, the additive power u_n that is required by the nth local generator to produce the additive power U_n in the localized power system is given by

$$u_n(t) = MU_n(t)/M_n \tag{12}$$

This power is in addition to P_{mn}. However, since this additive power is a negative quantity, it also means that $\Delta P_{en} = -u_n(t)$ is an equivalent additional electrical output power of the local generator. Therefore, the new electrical output power required by the local generator to stabilize its respective LPS is given by

$$P_{en}^{new} = P_{en} + \Delta P_{en} \tag{13}$$

Other details can be found in [23] and [34].

In this investigation, the value of $\dot{\omega}$ required to estimate P_T and the value of ω required in OAS at the beginning of a time-step have been determined from the derivatives of a third degree polynomial approximation obtained by matching the LPS angle at current time and the LPS angles at three previous times. Note that this estimation process has not been used for estimation at future times. Assuming that the measurement data and hence the LPS angle δ was available at the beginning of the post-fault configuration, there was a delay of three time-steps to initiate the first local control action. At the beginning of a current time step after three previous time-steps in the post-fault configuration, the additive power controls required at different local generators were computed by OAS and they were then applied over the entire length of the current time-step.

The test results for a number of three-phase short-circuit faults are presented. Since the SBS method is the most accurate method, the CCT ranges for these fault cases were determined by the SBS method using COA frame. In each fault case, the CCT ranges were obtained without and with local controls applied. SBS trajectories corresponding to the critically stable conditions with local controls applied are also presented for each of these fault cases. However, the necessary power control at a local generator was achieved by applying Static Synchronous Series Compensator (SSSC). For this purpose, a single boundary bus is chosen arbitrarily at the local generator site such that this bus separates the rest of the system from the local network. For the local sites of generators 1-9, the high tension side of the step-up transformer is taken as the boundary bus, but for the local site of generator 10, the generator external bus is taken as the boundary bus due to the absence of step-up transformer.

However, since SSSC is a series FACTS device, a new bus is created to connect the SSSC between this new bus and the boundary bus. Therefore, the general setup with SSSC is shown in Fig. 4.

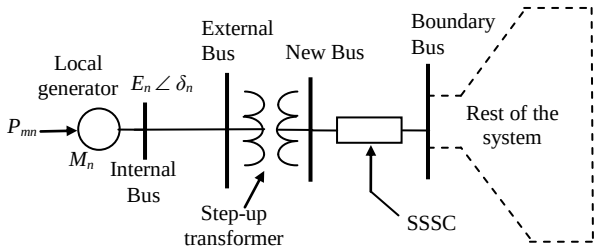

Fig. 4. Power System at the site of *n*th local generator with SSSC connected.

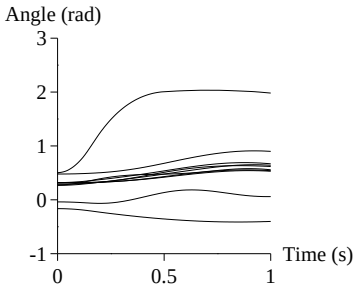

Fig. 5. SBS trajectories for fault case 1 at FCT of 0.15 s with local controls applied.

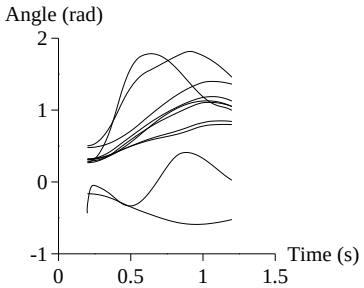

Fig. 6. SBS trajectories for fault case 2 at FCT of 0.20 s with local controls applied.

Fault Case 1: A three-phase short circuit fault on bus 29 was cleared by removing line 29-26, i.e. the line connected between the bus 29 and bus 26. Without any local control applied, the system was found to be stable at a fault clearing time of 0.07 s and unstable at a fault clearing time of 0.08 s. So the CCT range without local controls applied was (0.07 s to 0.08 s). However, with local controls applied, the system was found to be stable at a fault clearing time of 0.15 s and unstable at a fault clearing time of 0.16 s. Therefore, the CCT range with local controls applied improved to (0.15 s to 0.16 s). This is a very significant improvement. The SBS trajectories corresponding to the critically stable condition for this fault i.e. at the fault clearing time (FCT) of 0.15 s with local controls applied are shown in Fig. 5.

Fault Case 2: A three-phase short circuit fault on bus 25 was cleared by removing line 25-2. Without any local control applied, the CCT range was found to be (0.13 s to 0.14 s). However, with local controls applied, the CCT range improved to (0.20 s to 0.21 s). This is also a very significant improvement. The SBS trajectories corresponding to the critically stable condition for this fault i.e. at the FCT of 0.20 s with local controls applied are shown in Fig. 6.

Fault Case 3: A three-phase short circuit fault on bus 22 was cleared by removing line 22-21. Without any local control applied, the CCT range was found to be (0.17 s to 0.18 s). However, with local controls applied, the CCT range improved to (0.26 s to 0.27 s). The SBS trajectories corresponding to the critically stable condition for this fault i.e. at the FCT of 0.26 s with local controls applied are shown in Fig. 7.

Fault Case 4: A three-phase short circuit fault on bus 27 was cleared by removing line 27-17. Without any local control applied, the CCT range was found to be (0.18 s to 0.19 s). However, with local controls applied, the CCT range improved to (0.27 s to 0.28 s). The SBS trajectories corresponding to the critically stable condition for this fault i.e. at the FCT of 0.27 s with local controls applied are shown in Fig. 8.

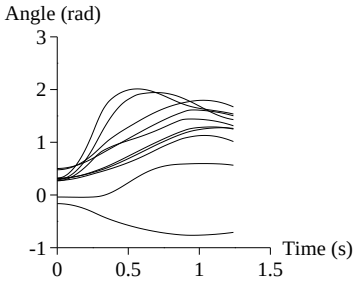

Fig. 7. SBS trajectories for fault case 3 at FCT of 0.26 s with local controls applied.

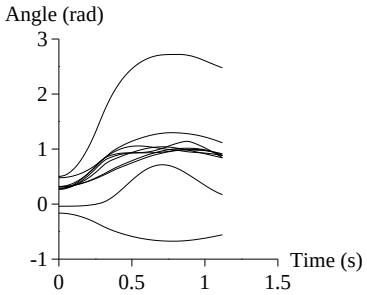

Fig. 8. SBS trajectories for fault case 4 at FCT of 0.27 s with local controls applied.

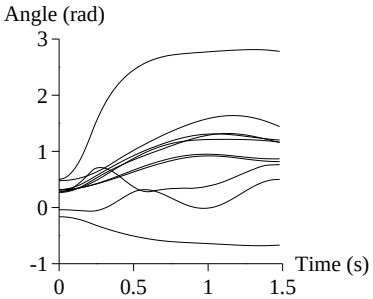

Fig. 9. SBS trajectories for fault case 5 at FCT of 0.20 s with local controls applied.

Fault Case 5: A three-phase short circuit fault on bus 26 was cleared by removing line 26-25. Without any local control applied, the CCT range was found to be (0.12 s to 0.13 s). However, with local controls applied, the CCT range improved to (0.20 s to 0.21 s). The SBS trajectories corresponding to the critically stable

condition for this fault i.e. at the FCT of 0.20 s with local controls applied are shown in Fig. 9.

Fault Case 6: A three-phase short circuit fault on bus 24 was cleared by removing line 24-23. Without any local control applied, the CCT range was found to be (0.20 s to 0.21 s). However, with local controls applied, the CCT range improved to (0.26 s to 0.27 s). The SBS trajectories corresponding to the critically stable condition for this fault i.e. at the FCT of 0.26 s with local controls applied are shown in Fig. 10.

Fault Case 7: A three-phase short circuit fault on bus 2 was cleared by removing line 2-1. Without any local control applied, the CCT range was found to be (0.16 s to 0.17 s). However, with local controls applied, the CCT range improved to (0.21 s to 0.22 s). The SBS trajectories corresponding to the critically stable condition for this fault i.e. at the FCT of 0.21 s with local controls applied are shown in Fig. 11.

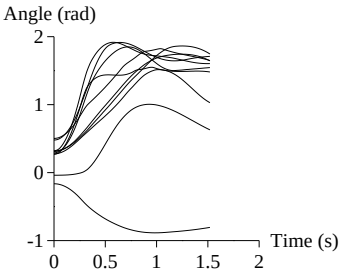

Fig. 10. SBS trajectories for fault case 6 at FCT of 0.26 s with local controls applied.

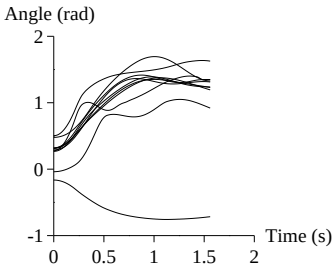

Fig. 11. SBS trajectories for fault case 7 at FCT of 0.21 s with local controls applied.

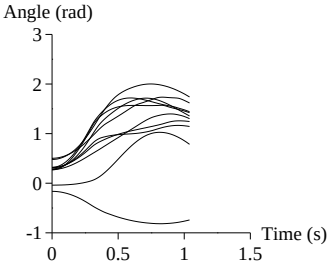

Fig. 12. SBS trajectories for fault case 8 at FCT of 0.28 s with local controls applied.

Fault Case 8: A three-phase short circuit fault on bus 15 was cleared by removing line 15-14. Without any local control applied, the CCT range was found to be (0.23 s to 0.24 s). However, with local controls applied, the CCT range improved to (0.28 s to 0.29 s). The SBS trajectories corresponding to the critically stable condition for this fault i.e. at the FCT of 0.28 s with local controls applied are shown in Fig. 12.

All the results presented here are summarized in Table I. The results show very good improvement of transient stability in terms of CCT ranges. These results clearly demonstrate the high potential of the real-time localized control of transient stability by the LTS method.

TABLE I. CCT RANGES WITHOUT AND WITH LOCALIZED CONTROL

Fault Cases	CCT Range (s) without Control	CCT Range (s) with Control
Fault Case 1	0.07-0.08	0.15-0.16
Fault Case 2	0.13-0.14	0.20-0.21
Fault Case 3	0.17-0.18	0.26-0.27
Fault Case 4	0.18-0.19	0.27-0.28
Fault Case 5	0.12-0.13	0.20-0.21
Fault Case 6	0.20-0.21	0.26-0.27
Fault Case 7	0.16-0.17	0.21-0.22
Fault Case 8	0.23-0.24	0.28-0.29

IV. CONCLUSIONS

Real-time localized control of transient stability by the Localized Transient Stability (LTS) Method with Static Synchronous Series Compensator (SSSC) as the local control means has been presented. In this technique, the post-fault power system is represented by a two-generator localized power system at the site of each individual generator. Each of these localized power systems is then driven to its respective stable equilibrium by local control actions with local computations using the locally measured data to drive the full (entire) power system to its stable equilibrium. However, since the technique is based on the LTS method, this technique overcomes the serious drawbacks of the different localized control strategies proposed in the literature. The test results presented here clearly demonstrate the high potential of real-time localized control of transient stability by the LTS method. However, further investigation of real-time localized control of transient stability by the LTS method using the other control strategies (i.e. control strategies other than the optimal aim strategy) with different local control means is necessary.

ACKNOWLEDGMENT

The material presented here is based upon work that is supported by the National Institute of Food and Agriculture, U.S. Department of Agriculture, Evans-Allen project number SCX-313-02-15.

REFERENCES

[1] A. A. Fouad and V. Vittal, *Power System Transient Stability Using the Transient Energy Function Method*, Prentice-Hall, 1992.

[2] Y. Xue, T. V. Cutsem, and M. Ribbens-Pavella, "Extended equal area criterion: justification, generalizations, applications," *IEEE Trans. Power Systems*, vol. 4, no. 1, pp. 44-52, February 1989.

[3] V. Vittal, P. Sauer, S. Meliopoulos, and G. K. Stefopoulos, "On-line transient stability assessment scoping study," Final Project Report, PSERC Publication 05-04, Power Systems Engineering Research Center (PSERC), 2005.

[4] A. M. Miah, "Study of a coherency-based simple dynamic equivalent for transient stability assessment," *IET Generation, Transmission & Distribution*, vol. 5, no. 4, pp. 405-416, April 2011.

[5] A. M. Miah, "Comparative study on the performance of a coherency-based dynamic equivalent with the new inertial aggregation," *Int. Journal of Applied Power Engineering*, vol. 1, no. 3, pp. 105-114, December 2012.

[6] A. M. Khalil and R. Iravani, "A dynamic coherency identification method based on frequency deviation signals," *IEEE Trans. Power Systems*, vol. 31, no. 3, pp. 1779-1787, May 2016.

[7] N. Yorino, E. Popov, Y. Zoka, Y. Sasaki, and H. Sugihara, "An application of critical trajectory method to BCU problem for transient stability studies," *IEEE Trans. Power Systems*, vol. 28, no. 4, pp. 4237-4244, November 2013.

[8] S. Zhao, H. Jia, D. Fang, Y. Jiang, and X. Kong, "Criterion to evaluate power system online transient stability based on adjoint system energy function," *IET Generation, Transmission & Distribution*, vol. 9, no. 1, pp. 104-112, January 2015.

[9] T. L. Vu and K. Turitsin, "Lyapunov functions family approach to transient stability assessment," *IEEE Trans. Power Systems*, vol. 31, no. 2, pp. 1269-1277, March 2016.

[10] F. Milano, "Semi-implicit formulation of differential-algebraic equations for transient stability analysis," *IEEE Trans. Power Systems*, vol. 31, no. 6, pp. 4534-4543, November 2016.

[11] M. Oluic, M. Ghandhari, and B. Berggren, "Methodology for rotor angle transient stability assessment in parameter space," *IEEE Trans. Power Systems*, vol. 32, no. 2, pp. 1202-1211, March 2017.

[12] H. Bosetti and S. Khan, "Transient stability in oscillating multi-machine systems using Lyapunov vectors," *IEEE Trans. Power Systems*, vol. 33, no. 2, pp. 2078-2086, March 2018.

[13] V. Jalili-Marandi, Z. Zhou, and V. Dinavahi, "Large-scale transient stability simulation of electrical power systems on parallel GPUs," *IEEE Trans. Parallel & Distributed Systems*, vol. 23, no. 7, pp. 1255-1266, July 2012.

[14] Y. Liu and Q. Jiang, "Two-stage parallel waveform relaxation method for large-scale power system transient stability simulation," *IEEE Trans. Power Systems*, vol. 31, no. 1, pp. 153-162, January 2016.

[15] M. A. Tomim, J. R. Marti, and J. A. P. Filho, "Parallel transient stability simulation based on multi-area Thevenin equivalents," *IEEE Trans. Smart Grid*, vol. 8, no. 3, pp. 1366-1377, May 2017.

[16] J. C. Cepeda, J. L. Rueda, D. G. Colome, and D. E. Echeverria, "Real-time transient stability assessment based on center-of-inertia estimation from phasor measurement unit records," *IET Generation, Transmission and Distribution*, vol. 8, no. 8, pp. 1363-1376, August 2014.

[17] S. Dusgupta, M. Paramasivam, U. Vaidya, and V. Ajjarapu, "PMU-based model-free approach for real-time rotor angle monitoring," *IEEE Trans. Power Systems*, vol. 30, no. 5, pp. 2818-2819, September 2015.

[18] Y. Wu, M. Musavi, and P. Lerley, "Synchrophasor-based monitoring of critical generator buses for transient stability," *IEEE Trans. Power Systems*, vol. 31, no. 1, pp. 287-295, January 2016.

[19] P. Bhui and N. Senroy, "Real-time prediction and control of transient stability using transient energy function," *IEEE Trans. Power Systems*, vol. 32, no. 2, pp. 923-934, March 2017.

[20] M. Glavic, D. Ernst, D. Ruiz-Vega, L. Wehenkel, and M. Pavella, "E-SIME – A method for transient stability closed-loop emergency control: Achievements and prospects," in *Proc. iREP Symposium - Bulk Power System Dynamics and Control - VII. Revitalizing Operational Reliability*, Charleston, South Carolina, USA, August 19-24, 2007, pp. 1-10.

[21] G. C. Zweigle and V. Venkatasubramanian, "Wide-area optimal control of electric power systems with application to transient stability for higher order contingencies," *IEEE Trans. Power Systems*, vol. 28, no. 3, pp. 2313-2320, August 2013.

[22] J. Zaborszky, A. K. Subramanian, T. J. Tran, and K. M. Lu, "A new state space for emergency control in the interconnected power system," *IEEE Trans Automatic Control*, vol. 22, no. 4, pp. 505-517, August 1977.

[23] J. Meisel and R. D. Barnard, "Transient-stability augmentation using a localized aiming-strategy algorithm," presented at Power System Computation Conf. V, Cambridge, England, paper no. 3.2/9, 1975.

[24] J. Meisel, A. Sen, and M. L. Gilles, "Alleviation of a transient stability crisis using shunt braking resistors and series capacitors," *Electrical Power & Energy Systems*, vol. 3, no. 1, pp. 25-37, January 1981.

[25] R. Patel, T. S. Bhatti, and D. P. Kothari, "Improvement of power system transient stability by coordinated operation of fast valving and braking resistor," *IEE Proc. Generation,* Transmission *and Distribution*, vol. 150, no. 3, pp.311-316, May 2003.

[26] M. H. Haque, "Improvement of first swing stability limit by utilizing full benefit of shunt FACTS devices," *IEEE Trans. Power Systems*, vol. 19, no. 4, pp. 1894-1902, November 2004.

[27] M. H. Haque, "Damping improvement by FACTS devices: A comparison between STATCOM and SSSC," *J. of Electric Power Systems Research*, vol. 76, no. 9-10, pp. 865-872, June 2006.

[28] M. H. Haque, "Application of UPFC to enhance transient stability limit," in *Proc. Power Engineering Society General Meeting*, Tampa, Florida, USA, June 24-28, 2007, pp. 1-6.

[29] A. M. Miah, "A new methodology for the purpose of real-time local control of transient stability," in *Proc. IEEE PES Transmission & Distribution Conference and Exposition*, Chicago, Illinois, USA, April 14–17, 2014, pp. 1-5.

[30] A. M. Miah, "Localized transient stability (LTS) method for real-time localized control," *Int. Journal of Applied Power Engineering*, vol. 7, no. 1, pp, 73-85, April 2018.

[31] A. M. Miah, "Real-time localized control of transient stability by the Localized Transient Stability (LTS) Method with Static Var Compensator (SVC)," in *Proc. Int. Conf. on Smart Grid and Clean Energy Technologies*, Malaysia, May 29–June 1, 2018, pp. 212-217.

[32] A. M. Miah, "Real-time localized control of transient stability," *Int. J. of Electrical and Electronic Engineering & Telecommunications*, vol. 7, no. 3, pp. 76-82, July 2018.

[33] R. D. Barnard, "An optimal-aim control strategy for nonlinear regulation systems," *IEEE Trans. Automatic Control*, vol. 20, no. 2, pp. 200-208, April 1975.

[34] A. M. Miah, "Local control of transient stability by optimal aim strategy," in *Proc. Third Int. Conf. on Electrical & Computer Engineering*, Dhaka, Bangladesh, December 28-30, 2004, pp. 171-174.

Abdul M. Miah received the B.Sc. and M.Sc. degrees in Electrical Engineering from the Bangladesh University of Engineering and Technology in 1969 and 1981 respectively, and the Ph.D. degree in electrical engineering from the Wayne State University, Michigan, USA, in 1992. He worked in industries for several years. He was also with the faculty of Bangladesh University of Engineering and Technology. He joined the South Carolina State University in 1990 and is currently a Professor of Electrical Engineering Technology. His current research interest is in the area of localized transient stability and control.